GEOLOGICAL STRUCTURES RELATIONSHIP OF JOINT, FAULT AND FOLD IN THE NORTH SERAYU MOUNTAINS IN THE TRAMBRA RIVER AREA, PURBALINGGA REGENCY, CENTRAL JAVA

A Widagdo[1]*, A Candra[1], H L Sunan[1]
[1] Geological Engineering, Universitas Jenderal Soedirman
Purwokerto, Central Java, Indonesia, 53123

Email : asmoro.widagdo@unsoed.ac.id

Abstract. The Tambra River as a research location is in the mountainous area of North Serayu, Purbalingga Regency, Central Java Province. The research was conducted to determine the relationship between various joint, fault and fold geological structures in the study area. The joint field data is in the form of strike and dip measurements of the joint plane. Fault field data in the form of strike and dip of fault plane, pitch angle, direction of pitch and type of fault movement. Fold data is carried out by measuring the layers of sedimentary rock layers that form anticline or syncline folds by measuring the strike and dip of the bedding plane. The results of the formation stress analysis show that the tectonic stress trending north-south forms rock fractures/joints, faults and folds in the study area.

Keywords: Geological structure, fault plane, pitch angle, joint plane

1. Introduction

The Tambra River area and its surroundings are on the southern side of the North Serayu Mountains. As part of the North Serayu Mountains, the study area has interesting geological dynamics due to orogenic processes that occurred on the island of Java. The arching up of the Java Geanticline, according to [1], which occurred in the Plio-Pleistocene is related to the anticline structure in the North Serayu Mountains. According to [2] stated that the Sunda Orogeny in the Late Neogene (Pliocene) caused folding of Miocene-Pliocene sediments in the north of Java Island, while in the south of Java Island this orogenesis caused old volcanic rocks to experience folding, faulting and uplift. Joints, faults and folds in this area need to be studied to determine the relationship between their formation genes and the resulting geological potential.

The Tambra River area has a mountainous morphology, where its formation is controlled by the tectonic process of uplift through folding and fault structures [3]. Old volcanic rock formations in this area have a relatively faster uplift rate than young sedimentary rocks [4]. Apart from forming the morphology, this tectonic activity also poses a potential threat of disaster in this area.

The location of the study area is in the central part of Java Island, in general it is an area that has the possibility of higher tectonic activity than other areas in the north and south of Java Island (Figure 1). This is indicated by various complex geological structural factors with intensive joints, faults and folds. The presence of a plate subduction zone in the south of Java Island makes this area an active tectonic boundary (Figure 1).

Physiographically, the study area is included in the Bogor-Serayu-Kendeng Anticlinorium [5]. The Bogor-Serayu-Kendeng Anticlinorium is a large fold consisting of small folds that are relatively west-east trending. The rocks that make up this landscape include rocks of Tertiary age (tens of millions of years ago) that are strongly folded with the main geological structures in the form of faults and folds.

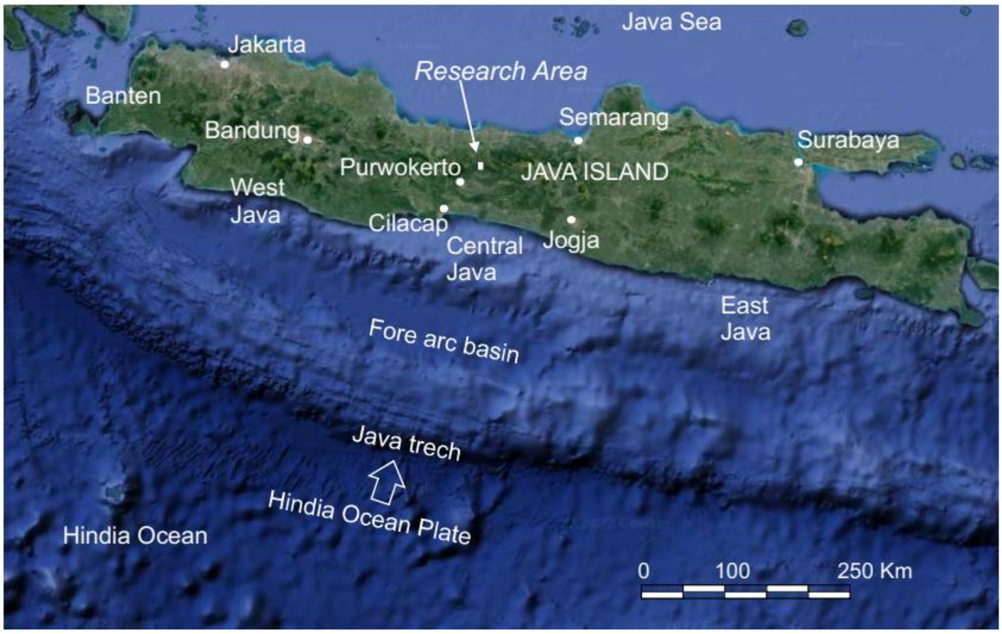

Figure 1. Location of the research area in the country of Indonesia's Central Java.

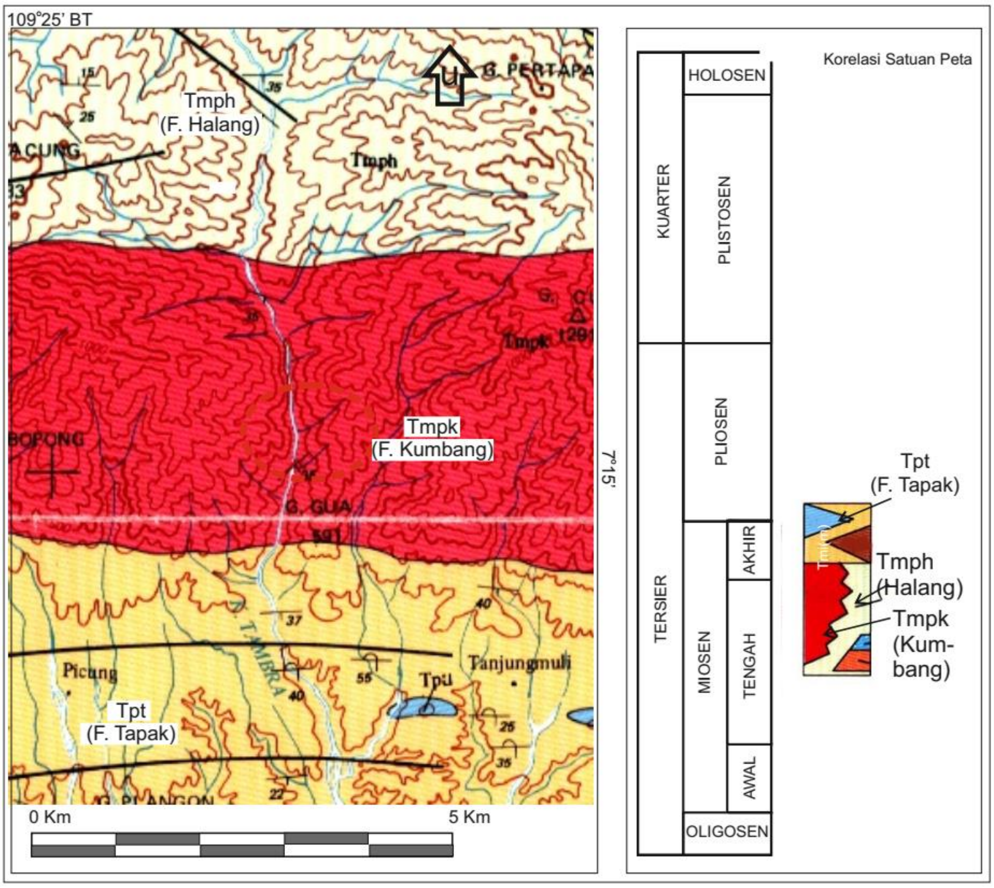

Figure 2. Regional geological map of the research area and its surroundings according to [6].

In terms of stratigraphy or sequence of rock formation, the research area and its surroundings are mainly composed of lithology/volcanic rocks and sediments of Tertiary age [6]. The Ramban Formation is composed of sandstone-carbonate rocks and conglomerates interbedded with thin layers of marl and shale in the lower part of the formation, while the upper part of the formation consists of light gray to bluish sandstone-limestone. Sandstone generally contains pieces of andesitic igneous rock. The Halang Formation is composed of sedimentary rocks in the form of sandstone, conglomerate, tuffan, marl and mudstone [7; 8] which are of Middle-Late Miocene age (around 15-5 million years ago).

The Kumbang Formation [6] is composed of volcanic-breccia rocks, lava, igneous intrusions, and tuffs of andesitic to basaltic composition; tuff sandstone and conglomerate, as well as inserts of thin layers of magnetite. This unit has an inter-fingering relationship with the Halang Formation (Figure 2). The Halang Formation [6] is composed of sandstone-tuffstone, conglomerate, marl, and mudstone; At the bottom there is breccia with an andesite rock composition. Sandstone is generally in the form of wakestone. This formation rock was deposited as a result of turbidite sedimentation in the upper bathyal zone (shallow sea). The Tapak Formation (Tpt) consists of greenish coarse-grained sandstone and conglomerate, locally found andesite breccia. The upper part consists of calcareous sandstone and green marl which contains many mollusk fossils. This Pliocene age formation (less than 1.8 million years ago) has a thickness of up to 500 meters [6].

The regional geological structure of the research area is anticlinal folds trending west-east. The Halang, Kumbang and Tapak formations in the study area are the southern flank of this fold. Thus, the slope of the rocks from these formations generally has a southerly direction.

2. Methods

At the field work stage, measurements of joints, faults and bedding areas were carried out as well as taking rock samples and observing lithology. The laboratory analysis stage includes analysis of joints, faults and rock bedding areas. Based on the overall results of this analysis, a synthesis was then prepared regarding the geological structure of the research area.

One way to determine ancient stresses is the joint structure as a result of brittle deformation. In order to determine the relationship between fracture and stress axes, it is important to determine the genetic class of fracture. Joints can take the form of tension fractures or shear fractures which may appear as conjugate pairs.

Measurement and identification of rock fractures or joints includes measuring the strike on the joint plane, measuring the dip of the joint plane and the direction of slope of the joint plane. Field data measurements use the righthand rule where the dip direction is to the right of the strike direction of the field being measured. When collecting/recording joint data in the field, the more data the more accurate it will be in producing conclusions. The joint data was grouped directly based on physical characteristics in the field (shear joints, tensional joints, hybrid joints and veins). Analysis of joint data was carried out using statistical methods which were carried out by drawing rosette diagrams and contour diagrams, using stereographic projections and polar projections.

Measurement and identification of rock bedding areas include strike measurements on rock bedding planes, measuring dipping of bedding planes. Field data measurements use the righthand rule where the dip of the rock bedding plane is to the right of the strike direction of the bedding plane being measured. Measurement of the strike and dip of these rock layers is carried out using a geological compass.

On the fault plane, strike, dip, pitch angle, pitch opening direction and type of movement are determined and measured. Fault data measurements were carried out with a geological compass and protractor directly on rocks in the field. Analysis was carried out to determine the main stress that forms the fault structure. The types of fault movement can be thrust, normal, dextral and sinistral movements.

3. Results And Discussion

Stratigraphically, the study area is composed of a Sandstone Unit with a Mudstone Insertion, a Volcanic Lava-Breccia Unit and a Carbonate Claystone Unit with a Sandstone Insertion. The Mudstone Insert Sandstone Unit is the oldest rock unit occupying the northern part of the study area. This rock unit is part of the upper Halang Formation in the study area.

The rock arrangement/stratigraphy at rock outcrops is composed of alternating layers of medium-fine grained sandstone and claystone. The sandstone is yellowish gray in color, fine to medium sand grain size, rather fragile with good sorting. In some parts, lamination and burrowing structures are found.

Based on megascopic field observations, the mudstone in the research area has a fresh brownish gray to dark brown color, is rich in organic material, and has a laminated structure. The sedimentary structure found in mudstone is lamination. The bedding areas found have a relative strike to the east and dip to the south. Based on their physical characteristics and lithological associations, the rocks in the study area are part of the Halang Formation.

Outcrops of basaltic lava were found in the central part of the study area which were exposed in a fresh to slightly weathered condition. The outcrops found in the drainage channel are predominantly fresh. The thickness of the unit is estimated to be approximately 1400 meters. These rocks are interpreted as Kumbang Formation rocks. Based on the dip of this rock, it points south. The structures found in the field are pillow structures and solid columns. This breccia is composed of fragments and matrix. Megascopically, this breccia has silica cement, a matrix in the form of glass like small fragments, floating fragments in the matrix, arranged monomically and basalt fragments. Light gray, aphanitic, massive basalt fragments, consisting of the mineral olivine, pyroxene, plagioclase. There are many outcrops of this breccia unit in the central part of the study area. These lava rocks and breccia are interpreted as part of the Kumbang Formation which has a Late Miocene age.

The Carbonate Claystone Unit with Sandstone Inserts occupies approximately 25% of the study area. Outcrops in this unit are found in the southern part of the research area which are exposed in a fresh to weathered condition. The outcrops found at the bottom of the river are in fresh condition. The thickness of this unit can be calculated from a geological cross section of >625 meters. These rocks are interpreted as part of the Tapak Formation which has a Pliocene age.

Shear joints in the study area develop intensively in sandstone as inserts in the more dominant mudstone (Figure 3). This is in accordance with the character of sandstone which is brittle, while claystone is more flexible or ductile. The stress acting on this rock will cause the compact sandstone to break, while the claystone will fold more to accommodate the compressive stress (Figures 3 and 4). On this rock, 45 data measurements were carried out (Table 1). In the field, this joint is recognized by its smooth, tight, long surface appearance and generally pairs at an angle of around 60 degrees. Bi-directional rose diagram analysis of a total of 45 data (Table 1) of shear fractures measured in the study area produces general directions of joints in the north-south and west-east directions (Figure 4). The contour diagram of the dip of the joint in the study area shows that the polar contour of the dip of the joint is especially darker in the south and east, this shows the dip of the joint, especially towards the west and north. Thus, the main compressional stress that forms joints can be interpreted as originating from the southeast-northwest direction.

Figure 3. Shear fractures with dense, smooth and paired surfaces.

Table 1. Shear fracture measurement data

No	Strike	Dip	No	Strike	Dip	No	Strike	Dip
1	275	52	16	265	65	31	240	55
2	170	57	17	122	72	32	145	70
3	276	75	18	275	68	33	150	75
4	280	50	19	260	70	34	285	75
5	170	52	20	255	73	35	190	85
6	165	60	21	276	72	36	300	82
7	170	55	22	280	77	37	154	55
8	270	45	23	272	77	38	252	55
9	280	75	24	255	80	39	345	70
10	282	55	25	263	70	40	345	67
11	285	58	26	165	65	41	350	86
12	260	70	27	255	60	42	240	58
13	260	57	28	170	60	43	355	54
14	265	70	29	262	47	44	240	68
15	258	80	30	250	55	45	315	70

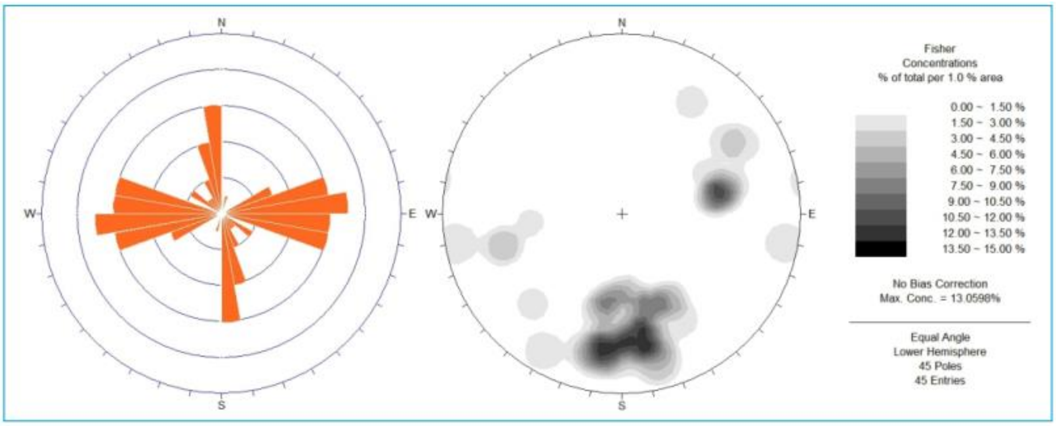

Figure 4. Rose diagram and shear joint plane contour diagram in the study area (n=45 data).

Figure 5. Tensile joints with rough, open and short surfaces in sandstone.

Table 2. Tensile joint/extension joint measurement data

No	Strike	Dip	No	Strike	Dip	No	Strike	Dip
1	220	52	16	350	80	31	5	82
2	220	27	17	10	85	32	30	85
3	273	58	18	12	82	33	210	85
4	260	60	19	12	80	34	330	65
5	10	80	20	350	80	35	345	70
6	5	80	21	355	82	36	30	80
7	170	80	22	350	84	37	25	85
8	240	22	23	305	55	38	28	85
9	277	45	24	355	60	39	20	80
10	242	82	25	2	85	40	345	85
11	90	25	26	205	68	41	350	86
12	130	30	27	320	80	42	260	70
13	275	45	28	355	82	43	175	80
14	100	58	29	5	80	44	350	80
15	186	89	30	335	80	45		

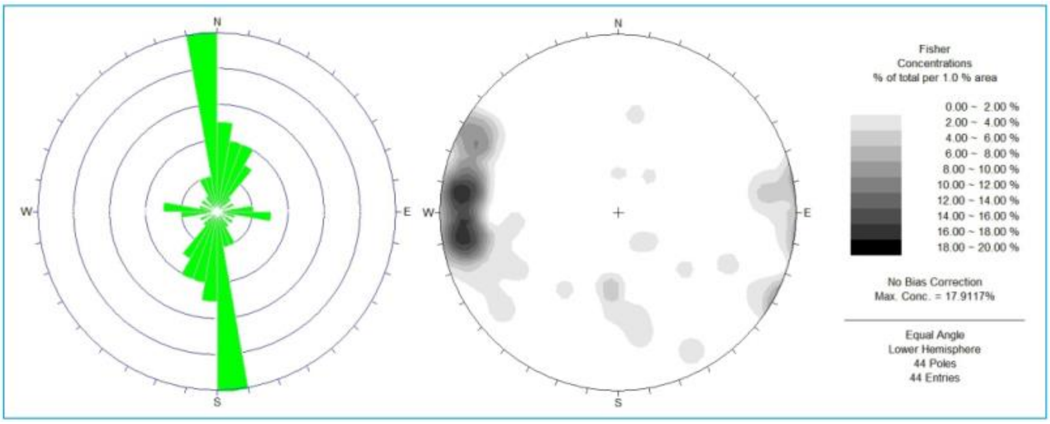

Figure 6. Rose diagram and contour diagram of tensile joints in the study area (n=44 data)

Extensional fractures in the study area, like shear fractures, develop intensively in sandstone (Figure 5). As with shear fractures, this is in accordance with the character of sandstone which is brittle, while claystone is more flexible or ductile. The stress acting on this rock will cause the compact sandstone to break, while the claystone will fold more to accommodate the compressive stress (Figure 5). On this rock, 44 data measurements were carried out (Table 2). These joints are recognized in the field by their rough, open, short surface appearance and are generally paired with other tensile joints forming an angle of around 90 degrees. Bi-directional rose diagram analysis of 44 data (Table 2) of measured tensile joints produces the general direction of joints in the north-south and west-east directions (Figure 6). In the tensile joint plane contour diagram, it shows that the polar contour of the dip of the joint is especially darker in the western part, this shows the slope of the joint, especially towards the east, with a steep angle approaching vertical. Thus, the main compressional stress that forms joints can be interpreted as originating from the south-southeast direction.

Fault data found in the study area are minor thrust faults and dextral faults/right slip faults (Table 3). The dip of the thrust fault points to the southwest with a strike of N145^{o}E and a Dip of 30^{o}. The pitch angle of this thrust fault is 80^{o}, opening towards the southwest. The dextral fault has a strike of 150^{o} and a dip of 80^{o}, with a pitch angle of 14^{o} opening towards the south.

Table 3. Fault plane measurement data

No	Strike	Dip	Pitch	Opening direction	Movement Type
1	145	30	80	SW (Southwest)	Thrust
2	150	80	14	S (South)	dextral

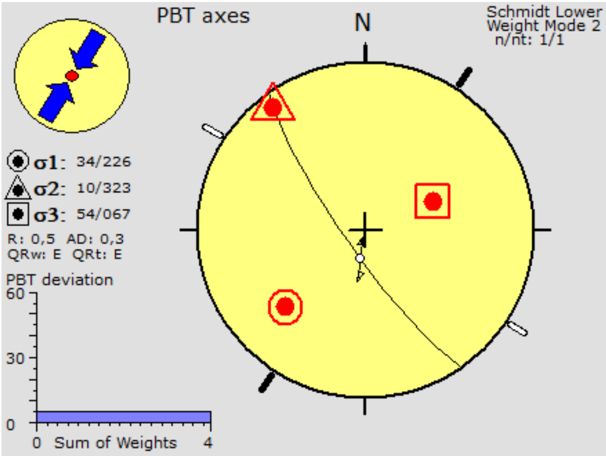

Figure 7. Stereographic analysis of thrust faults shows the influence of compressional stress from the southwest direction.

The results of stereographic analysis of thrust fault data show that this fault was formed by the main horizontal compressional force from the direction of 34°/N226°E or from the southwest direction with a plunge of 34° (Figure 7). The results of stereographic analysis of dextral fault data show that this fault was formed by the main horizontal compressional force from the direction 03°/N197°E or from the south-southwest direction with a plunge of 03° (Figure 8).

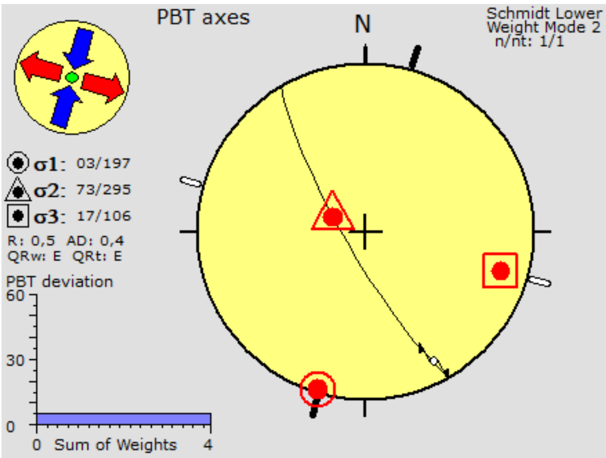

Figure 8. Stereographic analysis of dextral faults shows the influence of compressional stress from the south-southwest direction.

Table 4. Bedding plane of sedimentary rock measurement data.

No	Strike	Dip	No	Strike	Dip	No	Strike	Dip
1	30	42	12	85	35	23	60	25
2	47	30	13	260	36	24	70	45
3	10	25	14	80	65	25	65	45
4	65	52	15	92	47	26	66	28
5	55	32	16	115	35	27	95	33
6	87	42	17	92	36	28	110	45
7	85	42	18	92	47	29	94	50
8	90	20	19	94	56	30	96	52
9	95	40	20	86	50	31	99	52
10	92	55	21	88	44			
11	94	45	22	92	45			

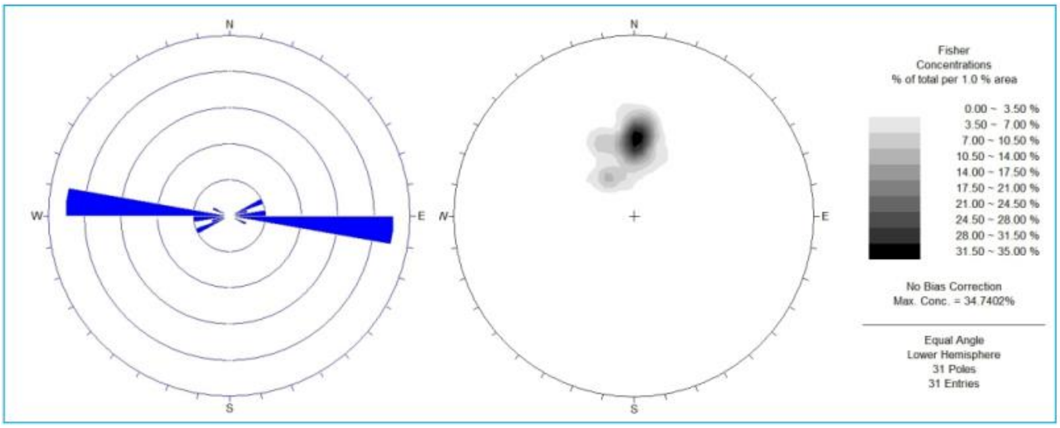

Figure 9. Rose diagram and contour diagram of sedimentary rock layers in the study area.

The rock bedding plane in the research area can be easily observed and measured. Layers of bedding can be easily observed at the boundary between mudstone and sandstone. Field measurements of bedding areas are mainly carried out at the boundaries of these rocks. On this bedding plane, 31 data measurements were made (Table 4) on the bedding plane. Bi-directional rose diagram analysis of 31 data (Table 4) of the measured bedding planes produces a general direction of bedding planes in the west-east direction (Figure 9). The contour diagram of the bedding plane shows that the polar contour of the dip of the bedding plane is especially darker in the north, this shows the slope of the bedding plane, especially towards the south, at an angle of around 45 degrees. Thus, the main force / compressional stress that forms the slope of the bedding plane can be interpreted as originating from the north-south direction.

The results of the analysis of the geological structure of joints, faults and bedding planes (as part of a fold) in the research area can be explained by the concept of structure formation according to the simple shear concept according to Harding (1974) as shown in Figure 10. North-south trending stress due to subduction in the south of Java Island produces pairs of scoured joints that form an acute angle to the maximum compressional stress. The dextral fault is a synthetic strike slip in Figure 10. The area of rock layers is part of a fold that trends east-west. Extension fractures trend North-South in the direction of maximum compressional stress.

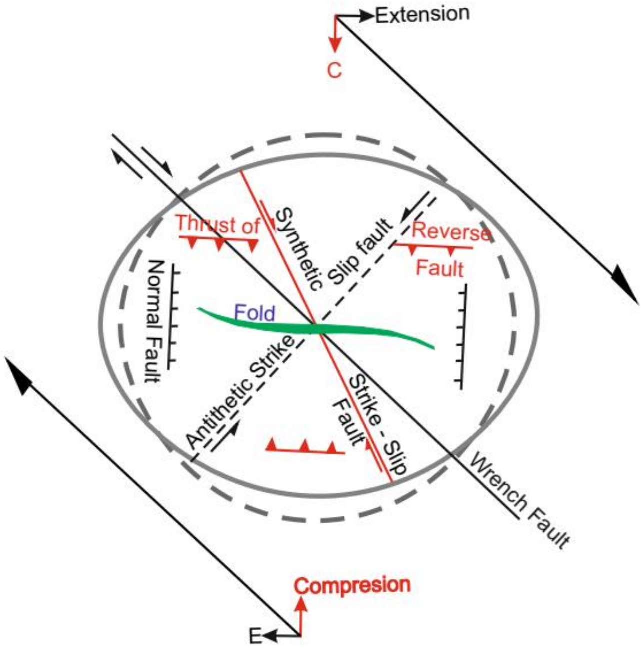

Figure 10. Formation of various geological structures based on the simple shear concept according to Harding (1974).

4. Conclusion

4.1. Nanoparticle formulation of EtOH extract from B. gymnorhiza F1 leaves using 200 mg carboxymethyl chitosan produces particles with the best physical properties.

4.2. F1 nanoparticles produce small and homogeneous particles, square in shape with a size of 196,5 ± 29,56 nm; The PI is 0,252 ± 0,053 and the zeta potential is -17,43 ± 1,01 mV. The results of FT-IR analysis show that there are similar functional groups between the nanoparticles and B gymnorhiza leaf extract.

References

[1]. Chali, B.U., Hasho, A. & Koricha, N.B. (2021) 'Preference and Practice of Traditional Medicine and Associated Factors in Jimma Town, Southwest Ethiopia', *Evidence-based Complementary and Alternative Medicine*, vol. 2021.

[2]. Dia, S.P.S., Nurjanah & Jacoeb, A.M. (2015) 'Chemical Composition, Bioactive Components and Antioxidant Activities from Root, Bark and Leaf Lindur', *Jurnal Pengolahan Hasil Perikanan Indonesia*, vol. 18, no. 2, pp. 205–19.

[3]. Hasnaeni, Wisdawati & Usman, S. (2019) 'The Effect of Extraction Method on Yield Value and Phenolic Content of Beta-Beta (Lunasia amara Blanco) Bark Extract', *Jurnal Farmasi Galenika* , vol. 5, no. 2, pp. 175–82.

[4]. Haq, M., Sani, W., Hossain, A.B.M.S., Taha, R.M. & Monneruzzaman K.M. (2011) 'Total phenolic contents, antioxidant and antimicrobial activities of Bruguiera gymnorrhiza', *Journal of Medicinal Plants Research*, vol. 5, no. 17, pp. 4112–8.

[5]. Saad, A.H.,dan Kadhim, R.D. 2011. Formulation and Evaluation of Herbal Mangroveo

from Zizhipus spina Leaves Extract. International Journal of Reseach in Ayurveda & Pharmacy. 2(6): 1802-1806.

[6]. Mahataranti, N., Astuti, I.Y., dan Asriningdhiani, B. 2012. Formulasi Mangrove Antiketombe Ekstrak Etanol Seledri (Apium graveolens L) dan Aktivitasnya terhadap Jamur Pytirosporum ovale. Pharmacy. 2 (09):128-139

[7]. Handayani, S. (2021) 'Aktivitas Antioksidan Ekstrak Hipokotil Bruguiera gymnorhiza Pada Pelarut Dan Fase Kematangan Yang Berbeda', *Agrointek : Jurnal Teknologi Industri Pertanian*, 15(3), pp. 685–694. Available at: https://doi.org/10.21107/agrointek. v15i3.8477.

[8]. Seepana, R., Perumal, K., Kada, N.M., Chatragadda, R., Raju, M. & Annamalai, V. (2016) 'Evaluation of antimicrobial properties from the mangrove Rhizophora apiculata and Bruguiera gymnorrhiza of Burmanallah coast, South Andaman, India', *Journal of Coastal Life*

[9]. Verma, A., Gautam, S., Bansal, K., Prabhakar, N. & Rosenholm, J. (2019) 'Green Nanotechnology: Advancement in Phytoformulation Research', *Medicines*, vol. 6, no. 1, p. 39.

[10]. Suhesti, T.S., Fudholi, A., Martien, R. and Martono, S., 2017, Pharmaceutical nanoparticle technologies: An approach to improve drug solubility and dissolution rate of Piroxicam, *Research J. Pharm. and Tech.*, **10**(4), 7 p. https://doi.org/ 10.5958/0974-360X.2017.00176.7

[11]. Suhesti, T.S., Fudholi, A., Martien, R., 2016, Application of Simplex Lattice Design for the Optimization of the Piroxicam Nanosupensions Formulation using Evaporative Antisolvent Technique, *IJPCR*, **8**(5)Suppl: p.433-439.

[12]. Rizvi, S.A.A. and Saleh, A.M. (2018)'Applications of nanoparticle systems in drug delivery technology', *Saudi Pharmaceutical Journal*, 26(1), pp. 64–70. Available at:https://doi.org/10.1016/j.jsps.2017.10.012.

[13]. Laili, H.N. and Winarti, L. (2014) 'Preparasi dan Karakterisasi Nanopartikel Kitosan-Naringenin dengan Variasi Rasio Massa Kitosan-Natrium Tripolifosfat', *e-Jurnal Pustaka Kesehatan*, 2(2), pp. 308–313.

[14]. Sardoiwala, M.N., Kaundal, B. and Roy Choudhury, S. (2018) 'Development of Engineered Nanoparticles Expediting Diagnostic and Therapeutic Applications Across Blood–Brain Barrier', in *Handbook of Nanomaterials for Industrial Applications*. Elsevier, pp. 696– 709. Available at: https://doi.org/10.1016/B978-0-12-813351-4.00038-9.

[15]. Hoang, N.H., Thanh, T. Le, Sangpueak, R., Treekoon, J., Saengchan, C., Thepbandit, W., Papathoti, N.K., Kamkaew, A. & Buensanteai, N. 2022, 'Chitosan Nanoparticles-Based Ionic Gelation Method: A Promising Candidate for Plant Disease Management', *Polymers*, vol. 14, no. 4.

[16]. Sari, R., Paramanandana, A., Isadiartuti, D. & Rahayyu, A.M. (2020) 'Pengaruh Jumlah Polimer terhadap Karakteristik Fisik dan Pelepasan Nanopartikel Fraksi Diterpen Lakton Sambiloto-Kitosan, *Jurnal Sains Farmasi & Klinis*, vol.7, no.2, p. 99.

[17]. Jain, A.K. and Thareja, S. (2019) '*In vitro* and *in vivo* characterization of pharmaceutical nanocarriers used for drug delivery', *Artificial Cells, Nanomedicine, and Biotechnology*, 47(1), pp. 524–539. Available at: https://doi.org/10.1080/21691401.2018.1561457.

[18]. Danaei, M., Dehghankhold, M., Ataei, S., Hasanzadeh Davarani, F., Javanmard, R., Dokhani, A., Khorasani, S. & Mozafari, M.R. (2018) 'Impact of particle size and polydispersity index on the clinical applications of lipidic nanocarrier systems', *Pharmaceutics*, MDPI AG.

[19]. Rahat, I., Imam, S.S., Rizwanullah, Md., Alshehri, S., Asif, M., Kala, C. and Taleuzzaman, M. (2021) 'Thymoquinone-entrapped chitosan-modified nanoparticles: formulation optimization to preclinical bioavailability assessments', *Drug Delivery*, 28(1), pp. 973–984. Available at: https://doi.org/10.1080/10717544.2021.1927245.

[20]. Dewi, M.K., Chaerunisaa, A.Y., Muhaimin, M. & Joni, I.M. (2022) 'Improved Activity of Herbal Medicines through Nanotechnology', *Nanomaterials*, MDPI, *12*(22), 4073; https://doi.org/10.3390/nano12224073

[21]. Mourdikoudis, S., Pallares, R.M. & Thanh, N.T.K. (2018) 'Characterization techniques for nanoparticles: Comparison and complementarity upon studying nanoparticle properties', *Nanoscale*, vol. 10, no. 27, pp. 12871–934.

[22]. Mahbubul, I.M. (2019) 'Stability and Dispersion Characterization of Nanofluid', *Preparation, Characterization, Properties and Application of Nanofluid*, Elsevier, pp. 47–112.

[23]. Modena, M.M., Rühle, B., Burg, T.P. & Wuttke, S. (2019) 'Nanoparticle Characterization: What to Measure?', *Advanced Materials*, Wiley-VCH Verlag.

[24]. Vogel, R., Pal, A.K., Jambhrunkar, S., Patel, P., Thakur, S.S., Reátegui, E., Parekh, H.S., Saá, P., Stassinopoulos, A. & Broom, M.F. (2017) 'High-Resolution Single Particle Zeta Potential Characterisation of Biological Nanoparticles using Tunable Resistive Pulse Sensing', *Scientific Reports*, vol. 7, no. 1.

[25]. Dian, L., Yang, Z., Li, F., Wang, Z., Pan, X., Peng, X., Huang, X., Guo, Z., Quan, G., Shi, X., Chen, B., Li, G. & Wu, C. (2013) 'Cubic phase nanoparticles for sustained release of ibuprofen: Formulation, characterization, and enhanced bioavailability study', *International Journal of Nanomedicine*, vol. 8, pp. 845–54.

[26]. Takechi-Haraya, Y., Ohgita, T., Demizu, Y., Saito, H., Izutsu, K. and Sakai-Kato, K. (2022) 'Current Status and Challenges of Analytical Methods for Evaluation of Size and Surface Modification of Nanoparticle-Based Drug Formulations', *AAPS PharmSciTech*,23(5), p.150. Available at: https://doi.org/10.1208/s12249-022-02303-y.

[27]. Martien, R., Adhyatmika, A., Irianto, I. D., Farida, V., & Sari, D. P. 2012. 'Perkembangan Teknologi Nanopartikel Sebagai Sistem Penghantaran Obat'. Majalah Farmaseutik, 8(1), 133-144.